



Mechanism of arsenic poisoning on SCR catalyst of CeW/Ti and its novel efficient regeneration method with hydrogen

Xiang Li^a, Junhua Li^{a,*}, Yue Peng^a, Huazhen Chang^b, Tao Zhang^a, Shen Zhao^a, Wenzhe Si^a, Jiming Hao^a

^a State Key Joint Laboratory of Environment Simulation and Pollution Control, School of Environment, Tsinghua University, Beijing 100084, China

^b School of Environment and Natural Resource, Renmin University of China, Beijing 100872, China

ARTICLE INFO

Article history:

Received 22 September 2015
Received in revised form 1 November 2015
Accepted 26 November 2015
Available online 27 November 2015

Keywords:

NH₃-SCR
As poisoning
Regeneration
Surface acid sites
NO_x adsorbed species

ABSTRACT

Deactivation and regeneration of arsenic are studied on novel CeO₂–WO₃/TiO₂ for selective catalytic reduction (SCR) of NO_x with NH₃. It is found that the activity and N₂ selectivity of poisoned catalyst are inhibited immensely at the entire temperature range. The fresh, poisoned and regenerated catalysts are characterized using XRD, BET, XPS, H₂-TPR, NH₃-TPD, NO + O₂-TPD, in situ Raman and in situ DRIFTS. The characterization results indicate that the poisoning of arsenic decrease BET surface area, surface Ce³⁺ concentration and the amount of Lewis acid sites and adsorbed NO_x species but increase the reducibility and number of chemisorbed oxygen species. According to the in situ DRIFTS investigations, the adsorption of surface-adsorbed NH₃ and NO_x species is suppressed at low temperature, while the reactivity between surface-adsorbed NH₃ and NO is prohibited at high temperature. A novel H₂ reduction regeneration not only effectively removes arsenic from the poisoned catalysts, but promotes surface Ce³⁺/Ce⁴⁺ ratio and form new NO_x adsorptive sites. However, it also affects the chemical properties of catalyst such as crystalline Ce₂(WO₄)₃ forming, surface active oxygen species raise and loss of Brønsted acid sites.

© 2015 Published by Elsevier B.V.

1. Introduction

Selective catalytic reduction (SCR) with NH₃ as an effective method for controlling NO_x emissions, has been widely used in recent decades [1–3]. The traditional V₂O₅–WO₃(MoO₃)/TiO₂ catalysts, as the core of SCR technology, have been commercially used on stationary source applications especially on coal-fired power plants since the 1970s. [1–5] However, some inevitable problems still exist in this catalyst system: the environmental toxicity of vanadium species, the high working temperature and oxidation rate of SO₂ to SO₃, and the low N₂ selectivity because of N₂O formation. After considerable comparison and screening, it is considered that cerium-based catalysts are widely accepted as promising candidates due to their non-toxic, excellent oxygen storage–release capacity and outstanding redox properties in the NH₃-SCR reaction.

In recent years, many types of Ce-based catalysts were reported, such as Ce–Mn [6], Ce–P [7], Ce–Ti [8], Ce–W [9,10], Ce–Mo [11], Ce–Nb [12], Ce–Cu–Ti oxides [13], and Ce–Mn–Ti [14]. Among these Ce-based composite oxide catalysts, Ce–W/Ti with large BET surface

area and remarkable surface acidity presents the most excellent NH₃-SCR activity together with 100% N₂ selectivity in a broad temperature range even under an extremely high GHSV of 500,000 h⁻¹ [15]. In addition, considering its strong resistance to H₂O and SO₂, it can be a promising catalyst to substitute the toxic vanadium based catalysts for the control of NO_x emission on coal-fired power plants.

Heavy metal arsenic, existing as As₂O₃ or As₄O₆ in the flue gas with concentrations between 1 μg/m³ and 10 mg/m³ depending on coals and furnaces, is a dangerous poison for commercial SCR catalysts [16]. Presently, several works regarding the role of arsenic in the deactivation process have been reported. Part of them have argued that gaseous As₂O₃ or its dimer As₄O₆ could diffuse into the catalyst and block up the micropore of catalysts; others have held that arsenic with high oxidation state could react with vanadium oxide to destroy the surface acid sites [16–18]. However, their works only focus on conventional V-based catalysts, and few works have systematically elucidated the influences on surface acidity, reducibility, and reaction mechanism for As poisoned Ce-based catalysts. Therefore, to better improve the applicability of Ce–W/Ti catalyst, it is necessary to investigate the effect of As on Ce–W/Ti catalysts.

The regeneration of deactivated catalysts is an economic, recyclable and environmentally friendly choice for reusing vast waste

* Corresponding author. Fax: +86 10 62771093.
E-mail address: lijunhua@tsinghua.edu.cn (J. Li).

catalysts. Therefore, simple, inexpensive and high-efficiency reactivated method is urgent and worth studying. Hot water, diluted H_2SO_4 and electrophoresis treatments used on alkali metal deactivated V-based catalysts are proved to be effective methods to remove poisons and recover the reaction activity of the catalysts [19,20]. Additionally, previous studies demonstrate that arsenic on the surface of catalysts can be oxidized and dissolved using 4% H_2O_2 solutions for commercial catalysts [21]. But some of the active components such as V, W and SO_4^{2-} are simultaneously removed under an H_2O_2 environment, which leads to restore the catalytic activity to a low degree. As a consequence, new methods for efficient arsenic removal are significant to be developed and explored.

In this study, As poisoned and H_2 reduction regenerated CeO_2-WO_3/TiO_2 catalysts are synthesized, studied and compared with fresh catalysts. Various characterizations related to structure changes, redox property, surface acidity and reaction mechanism are investigated aiming to elucidate the deactivation mechanism and regeneration efficacy. Moreover, we also try to clarify the relationship between surface species and catalytic reaction, and evaluate the advantages and disadvantages of regeneration method.

2. Experimental

2.1. Catalysts preparation, poisoning and regeneration

The CeO_2-WO_3/TiO_2 (Ce–W/Ti) catalysts were prepared by impregnation of anatase TiO_2 with appropriate amounts of ammonium metatungstate and cerium nitrate solutions, and $(NH_4)_2CO_3$ was used as precipitator. After being impregnated for 4 h, the mash was filtered, followed by subsequent washing with DI water for several times, drying overnight at 120 °C, and calcination at 500 °C for 4 h. The samples were expressed as CWT, where molar ratio of Ce to W to Ti was 2:1:7. The corresponding poisoned samples were obtained by impregnating of sample in As_2O_3 solutions with different concentrations followed by drying and calcination at 450 °C for 3 h. The poisoned samples were denoted as CWT_x, where x represented the As_2O_3 mass percentage, and their concentrations detected by XRF were presented in Table S2. The CWT_{A3} catalysts were chosen for reactivation in simple self-manufacture device under 10% H_2/Ar atmosphere at a heating rate of 10 °C min⁻¹ from 50 °C to 600 °C. The detailed instrument is shown in Fig. S1, and the regenerated sample was denoted as R600.

2.2. Catalysts activity

The activity tests were performed in a fixed-bed quartz reactor (I.D. = 6 mm) at atmospheric pressure. The reaction conditions were controlled as follows: 500 ppm NO, 500 ppm NH_3 , 3% O_2 , 200 ppm SO_2 (when used), 5% H_2O (when used), and N_2 as balance gas. The total flow rate and the gas hourly space velocity (GHSV) were 200 mL min⁻¹ and 120,000 mL g⁻¹ h⁻¹, respectively. Outlet gases concentrations of NO, NO_2 , NH_3 , and N_2O were monitored using an FTIR spectrometer (GASMET DX-4000). The results for steady-state activity of catalysts were recorded after about 20 min at each temperature. The NO_x conversion, N_2 selectivity and the pseudo-first order kinetic parameters were calculated according to the following equation [2]:

$$NO_x\text{conversion} = \frac{[NO_x]_{\text{inlet}} - [NO_x]_{\text{outlet}}}{[NO_x]_{\text{inlet}}} \times 100\% \quad (1)$$

$$N_2\text{selectivity} = \left(1 - \frac{2[N_2O]_{\text{outlet}}}{[NO_x]_{\text{inlet}} + [NH_3]_{\text{inlet}} - [NO_x]_{\text{outlet}} - [NH_3]_{\text{outlet}}} \right) \times 100\% \quad (2)$$

$$k = -\frac{F}{W} \ln(1 - x) \quad (3)$$

where F is the total flow rate (cm³ s⁻¹), W is the weight of the catalyst (g) and x is the relative NO_x conversion.

2.3. Catalyst characterization

The N_2 sorption isotherm of the samples was carried out at 77 K with a Micromeritics ASAP 2020 apparatus. The crystal structure was recorded on a powder X-ray diffractometer (Rigaku, D/max-2200/PC, Japan) between 10° and 65° at a step rate of 5° min⁻¹ using $Cu K\alpha$ ($\lambda = 0.15405$ nm) radiation. X-ray photoelectron spectroscopy (XPS) was performed with an ESCALab220i-XL electron spectrometer from VG Scientific using 300 W $Mg K\alpha$ radiations. And the binding energies were calibrated using the C 1s line at 284.8 eV as an internal standard. Temperature programmed reduction with H_2 (H_2 -TPR) experiments were performed on a chemisorption analyzer (Micromeritics, ChemiSorb 2720 TPX) under a 10% H_2/Ar gas flow (50 mL min⁻¹) at a rate of 10 °C min⁻¹ up to 900 °C after pretreatment at 300 °C in Ar for 1 h. The total H_2 consumption was calculated and calibrated by standard CuO sample.

Temperature programmed desorption (TPD) of NH_3 and $NO + O_2$ were carried out using a FTIR spectrometer (MKS, MultiGas 2030HS) to detect NH_3 , N_2O , NO and NO_2 . After pretreated at 350 °C in N_2 flow at 200 mL min⁻¹ for 1 h, the samples were cooled down to 100 °C and saturated with 500 ppm NH_3 or 500 ppm $NO + 3\%O_2$ until adsorption saturation, followed by N_2 purging at the same temperature to remove physical absorption species. The desorption of nitrogen-containing species was then performed in the range of 100–700 °C at a speed of 10 °C min⁻¹.

In situ DRIFTS (diffuse reflectance infrared Fourier transform spectroscopy) were measured on an FTIR spectrometer (Nicolet NEXUS 6700) equipped with a Smart Collector and an MCT/A detector. And the spectra were recorded by accumulating 32 scans with a resolution of 4 cm⁻¹. While in situ Raman spectra were recorded using a Raman microscope (InVia Reflex, Renishaw) equipped with a deep-depleted thermoelectrically cooled charge-coupled device (CCD) array detector and a high-grade Leica microscope. And the 532 nm line of the laser was used for recording the Raman spectra. Prior to each experiment, the catalyst was preheated at 400 °C for 1 h in flowing N_2 at a flow of 100 mL min⁻¹. The gas used for the in situ IR spectroscopy experiment was a mixture of 500 ppm NH_3/N_2 , 500 ppm NO/N_2 and 5% O_2/N_2 with a total flow rate of 50 cm³ min⁻¹, while for the in situ Raman spectroscopy experiment was 10% H_2/Ar .

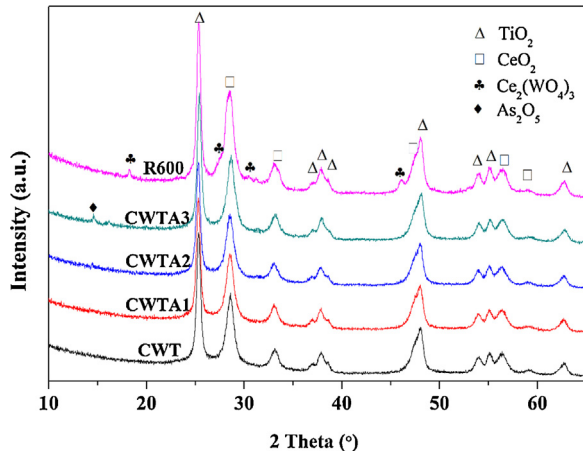
3. Results

3.1. Structural and textural characteristics (XRD, Raman and N_2 -physorption)

Fig. 1 displays the XRD patterns of the fresh, poisoned and regenerated catalysts calcined at 500 °C. It can be seen that both the diffraction peaks attributed to cubic fluorite-type phase CeO_2 (PDF-ICDD34-0394) and the peaks attributed to anatase phase TiO_2 (PDF-ICDD21-1272) are detected on the fresh, poisoned and regenerated catalysts. No visible phase of WO_3 species can be observed, signifying that the WO_3 species are highly dispersed on the surface of anatase. Furthermore, the diffraction peaks of poisoned catalysts are shifted to high angle direction gradually compared with fresh and regenerated samples, indicating that As has been incorporated into the lattice of CeO_2 and TiO_2 to form uniform solid solutions (containing $-Ce-O-As-$ and $-Ti-O-As-$ species) maintaining the CeO_2 cubic fluorite-type and TiO_2 anatase structures. With increasing the As content, the peak belonged to As_2O_5 (PDF-ICDD34-0394) occurs, indicative of a transformation from amorphous structure to ordered crystallized structure. Because at low As concentra-

Table 1Structural parameters measured by N_2 adsorption, XRD and Raman.

Sample	BET (m^2/g)	Pore size (nm)	Pore volume (cm^3/g)	Crystallite size ^a (nm)	Crystallite size ^b (nm)	Position of F_{2g} (cm^{-1})
CWT	53.9	10.4	0.19	17.7	10.4	462
CWTA1	44.8	12.7	0.19	18	10	461
CWTA2	43.2	12.7	0.17	18.2	10	459
CWTA3	42.5	12.5	0.17	18.1	10	458
R600	46	14.9	0.17	18.1	8.4	461

^a Calculated by anatase (101).^b Calculated by CeO_2 (111).**Fig. 1.** The XRD patterns of the fresh, poisoned and regenerated CWT catalysts calcined at 500 °C.

tion, especially for the As monolayer coverage below 1, it is very dilute for fresh catalysts. Therefore, As oxide can be well dispersed, and amorphous phase form. While for higher As concentration, it is inevitable that excess As oxide gathers and form crystallized structure. After regeneration, the diffraction peak of As_2O_5 disappears, while a series of new diffraction peaks assigned to monoclinic $Ce_2(WO_4)_3$ appear at the corresponding positions, demonstrating that part of CeO_2 has been transformed into the form of crystalline $Ce_2(WO_4)_3$ after high temperature reduction. Compared with fresh catalysts, the CeO_2 crystallite sizes calculated by Scherrer equation of the poisoned and regenerated samples are smaller, while their TiO_2 crystallite sizes are almost unchanged as listed in **Table 1**. The decreased CeO_2 crystallite sizes may be caused by the introduction of As^{3+} or As^{5+} into the lattice of CeO_2 , and further inhibits the crystal growth of the cubic phase or leads to contraction and distortion of the lattice due to that the ionic radius of As^{3+} (0.58 Å) or As^{5+} (0.46 Å) is smaller than that of Ce^{4+} (0.87 Å). Finally, an obvious phase separation of $Ce_2(WO_4)_3$ from CeO_2 is observed for the regenerated catalysts, indicating that their thermal stability is not very good.

It is well known that Raman spectroscopy is a good way to detect the surface information of the catalysts, especially lattice oxygen vibrations of fluorite phases. As shown in **Fig. 2** left, the bands due to the anatase of the support are detected at 397, 514 and 638 cm^{-1} [22]. Besides, all the catalysts show CeO_2 characteristic bands centered at 462 cm^{-1} corresponding the F_{2g} vibration mode of the cubic fluorite structure, which can be viewed as a symmetric breathing mode of oxygen atoms around [23]. Obviously, the F_{2g} vibration model (CeO_2) of the poisoned catalysts shifts to low wavenumber direction slightly compared with fresh and regenerated one (**Table 1**), indicating that the introduction of As^{5+} can change the surface structure of CeO_2 phase to form $-Ce^{4+}-O-As^{5+}-$ species which correlates with XRD data. In the high band, the peak at 806 cm^{-1} attributed to W–O–W modes is observed for all the samples. Notably, the fresh sample exhibits a broad peak centered at

951 cm^{-1} with a shoulder at 902 cm^{-1} , which is assigned to a well-dispersed polytungstate phase [24]. With increasing As content, the shoulder associated with this peak exhibits a blue shift to a higher wavenumber, which may be indicative of As–O–W or interaction between As oxide and W oxide at high As loadings. For the regenerated catalyst, the peak at 951 cm^{-1} disappears and is replaced by a new band at around 933 cm^{-1} ($Ce_2(WO_4)_3$ species) [25]. Similar results have been proposed by Mamede et al. who have studied the characterization and reactivity of WO_x-CeO_2 catalysts [26]. They found that with increasing W loading and upon calcination at high temperature, the $Ce_2(WO_4)_3$ compound was formed. These results above indicate that doping with As varies the phase structures of CeO_2 and weakens the dispersions of active component WO_x species. Besides, the new $Ce_2(WO_4)_3$ phase occurs along with As wearing off after high temperature reduction regeneration.

N_2 adsorption–desorption isothermal plot and the corresponding textural data of the fresh, poisoned and regenerated samples are shown in **Fig. S2** and summarized in **Table 1**, respectively. The isotherms of these samples are of classical type IV (IUPAC) [27], which is characteristic of mesoporous materials. Additionally, a well-defined H3-type hysteresis loop is shown at high relative pressure range (P/P_0) for each sample. This H3-type hysteresis loop is typical for narrow mesoporous structure formed by sheet shaped nanoparticle assembly. As listed in **Table 1**, a remarkable decrease in the BET surface area and the pore volume are observed for poisoned catalysts, whereas the pore diameters remain nearly unchanged with As content increase. These can be ascribed to the blocking effect on pores arising from deactivation of As_2O_5 species.

3.2. Catalytic activity

The influence of different As additives and regeneration on the activity and selectivity of the $Ce-W/Ti$ catalyst is presented in **Fig. 3**. The NO_x conversion of fresh catalyst is maintained above 90% in a range of 250–500 °C even though the GHSV reached 120,000 h^{-1} . Whereas the inhibition effect of As_2O_5 on activity and selectivity can be observed over all poisoned catalysts with dramatically decreased NO_x conversions and increased N_2O production. Apparently, CWTA3 shows poor activity within the whole temperature range investigated, with the maximum NO_x conversion of only below 60%. Meanwhile its selectivity to N_2 decreases from 99% at 300 °C to 83% at 500 °C with a high N_2O production at 60 ppm. These indicate that arsenic has a great negative impact on the catalytic activity and N_2 selectivity of $Ce-W/Ti$ catalysts at whole temperature range, in accord with our previous study on VW/Ti catalysts [28,29]. In contrast, a clearly healing impact is obtained for the regenerated sample, and the maximum NO_x conversion reached to 90% at 300–400 °C accompany with little N_2O production. Although not as good as fresh sample, it is obvious that that high temperature H_2 reduction is a good way for As_2O_5 removal and reactivation for poisoned catalysts. In order to illuminate the poison effect of As on the catalytic temperature, NO transformation frequency per Ce atom at 200 and 350 °C for all catalysts are given in **Fig. 4**. The value decreases from 1.2 s^{-1} for fresh catalyst to 0.03 s^{-1} for CWTA3, almost 97.56% loss, at 200 °C; at the same time, it decreases by

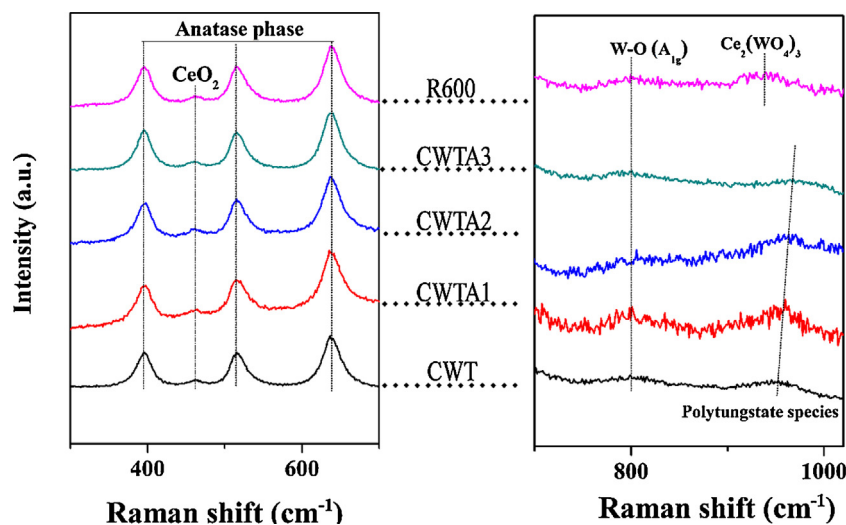
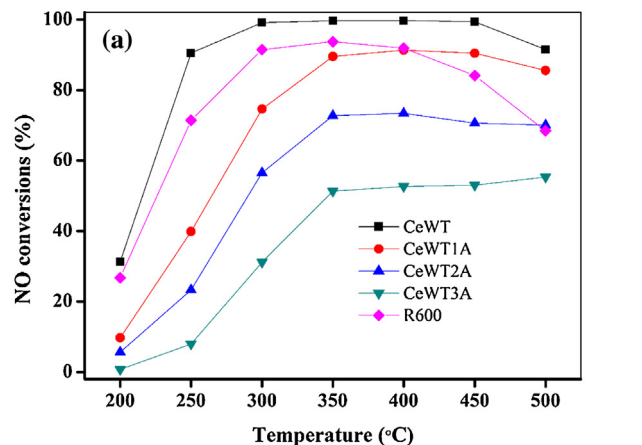


Fig. 2. Raman spectra of the fresh, poisoned and regenerated CeW/Ti catalysts calcined at 500 °C.

Fig. 3. (a) NO_x conversion and (b) N₂ selectivity and N₂O production of fresh, poisoned and regenerated CWT catalysts. Reaction condition: [NO] = [NH₃] = 500 ppm, [O₂] = 3%, N₂ balance, total flow rate = 200 mL/min, GHSV = 120000 h⁻¹.

50.01% when As₂O₅ mass concentration reaches to 3% at 350 °C. Thus, As has a far greater impact on catalytic performance at low temperature than at high temperature for Ce-W/Ti catalysts. And yet for all that, reduction regeneration make NO transformation frequency of poisoned sample recover to more than 80% no matter at low temperature or high temperature.

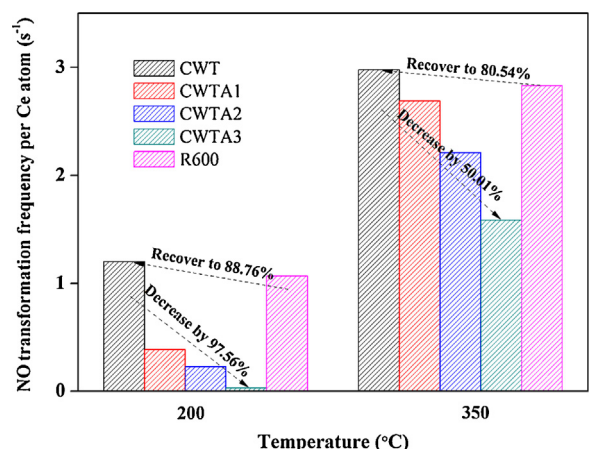


Fig. 4. Comparison of fresh, poisoned and regenerated CWT catalysts on NO transformation frequency at 200 °C and 350 °C.

SO₂ and H₂O are the two main components in the combustion exhaust from coal fired power plant, so it is very important to investigate the SCR activity in the presence of SO₂ and H₂O. As shown in Fig. S3, when 200 ppm of SO₂ and 5% H₂O are introduced over the whole reaction temperature range, the NO_x conversions for all catalysts decrease significantly at high GHSV (120,000 h⁻¹). Still, the Ce-W/Ti catalyst shows excellent H₂O and SO₂ durability for holding 90% NO_x conversion at 450–500 °C. While for CWTA3, the maximum value of NO_x conversion is only below 30%, which means that As has a greater suppression effect to catalytic activity under the condition with H₂O and SO₂. Additionally, N₂O production is barely detectable in this study, this may be attributed to the competitive adsorption of H₂O and NH₃ molecules on the acid sites and thus inhibiting NH₃ oxidation reaction [2]. All the results suggest that water vapor and sulfur dioxide have a negative effect for all the samples, especially for poisoned catalysts.

3.3. Reduction properties (H₂-TPR and *in situ* Raman)

H₂-TPR measurement is a good way to reflect both the reducibility of metal oxide catalysts (valence conversion) and the potential to remove or take up oxygen from peak position and hydrogen consumption. Fig. 5 presents the H₂-TPR profiles on fresh, poisoned, and regenerated Ce-W/Ti catalysts. The pristine Ce-W/Ti catalyst

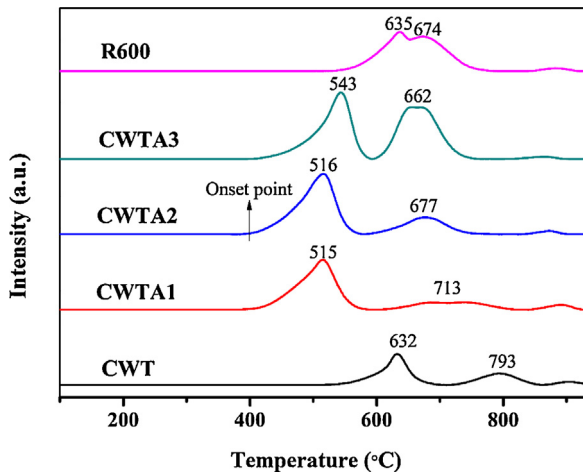


Fig. 5. H_2 -TPR profiles of the fresh, poisoned and regenerated CWT catalysts.

shows two apparent reduction peaks centered at 632 and 793 °C, assigned to the reduction of surface Ce^{4+} to Ce^{3+} and bulk Ce^{4+} (to Ce^{3+}) and W^{6+} (to W), respectively [24,30,31]. However, it is clear that the main reduction peaks of poisoned catalysts are larger than the fresh one, which hints a larger H_2 consumption due to the reduction of As species; simultaneously, an obvious shift toward lower temperatures is observed for both the two reductive peak with As content increase. Moreover, for CWTa3, the onset point and peak position of TPR curve slightly shift to the high temperature compared to the CWTa1 and CWTa2 peaks. According to the observation of As poisoned vanadium-based catalysts in previous reports and XRD data, these results are indicative of chemical environment changes of surface Ce^{4+} species and $\text{Ce}-\text{O}-\text{As}$ (W) bonds formation after a few As addition, due to As_2O_5 strong oxidizing property. But excess As introduced leads to ordered crystallized As_2O_5 structure formation as XRD profiles shown, which covers the catalyst surface. As a consequence, the reduction peaks of CWTa3 move toward high temperature direction.

In order to confirm our deduction, in situ Raman spectra of the TPR experiments of CWT and CWTa3 are carried out for the same conditions (Fig. 6). For the poisoned catalyst, the peak intensity of the CeO_2 decreases with increasing temperature from 350 °C to 450 °C, and its F_{2g} (triple degenerate state symmetry) vibration

model is undetectable at 500 °C. While the F_{2g} mode is still apparent at 500 °C and even at 600 °C. The results show a good agreement with the H_2 -TPR profile and indicate that doping with As could result in strong interaction between As species and Ce species and change of chemical environment of CeO_2 . In addition, according to the nucleation and contracting sphere models, the reduction of oxide occurred first on the surface and then progressively affects the bulk [32]. When hydrogen contact with the surface oxide, the reaction start and maintain for some time. Consequently, the reactants are totally covered by a layer of metal product, forming in the first instant of the reaction. hereafter, reaction interface begins to decrease, on account of the overlapping of the metal product and the reaction rate. Thus the reduction of the oxygen-containing ingredients inside the crystallite (inner bulk) become even more difficult, and smaller crystallite size is in favor of reduction reaction continuing. Trovarelli et al. had found that high temperature CeO_x reduction was strongly depended on its crystallite size, an obvious shift toward lower temperatures was observed for the high-temperature peak by reducing CeO_x crystallite size [33]. As shown above, the average crystallite size of CeO_2 decreases with addition of As, and thus a strong interaction between Ce and As evidenced by XRD and Raman can further improve the redox properties of CeO_2 .

Previous researchers also found that the H_2 reduction peaks below 700 °C could be associated with the reduction of surface capping oxygen, which is always responsible for the catalytic performance of the ceria-based catalyst [34,35]. In this study, we calculate both the H_2 consumption (<700 °C) per specific surface area ($\text{H}_2/S_{\text{BET}}$) over the CeW/Ti series catalysts. A good negative correlation between the $\text{H}_2/S_{\text{BET}}$ and k at 200 °C can be observed, as shown in Fig. S4. However, no certain correlations have been found between the $\text{H}_2/S_{\text{BET}}$ and relative concentration ratios of $\text{O}_\alpha/(\text{O}_\alpha + \text{O}_\beta)$ calculated by subsequent XPS results. These results suggest that the H_2 consumption peaks below 700 °C are mainly associated with the reduction of As_2O_5 content rather than surface capping oxygen over the poisoned and regenerated catalysts. Finally, the peak position (793 °C) belong to bulk Ce^{4+} (to Ce^{3+}) and W^{6+} (to W) of fresh sample shifts to the lower temperature (674 °C) for R600 after regeneration. A possible explanation is that part of bulk CeO_2 and WO_3 are changed into the $\text{Ce}_2(\text{WO}_4)_3$ compound species proved by XRD curves, more easier to be reduced, after high temperature reduction treatment.

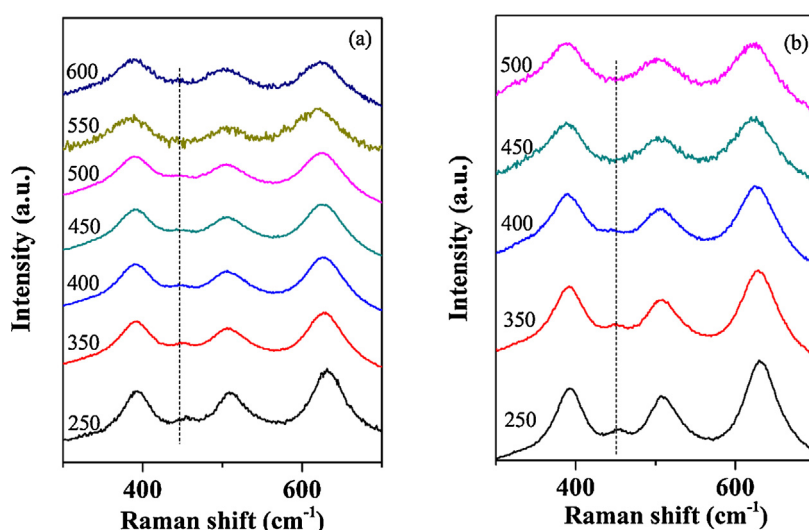


Fig. 6. In situ Raman spectra of the CWT (a) and CWTa3 (b) catalysts.

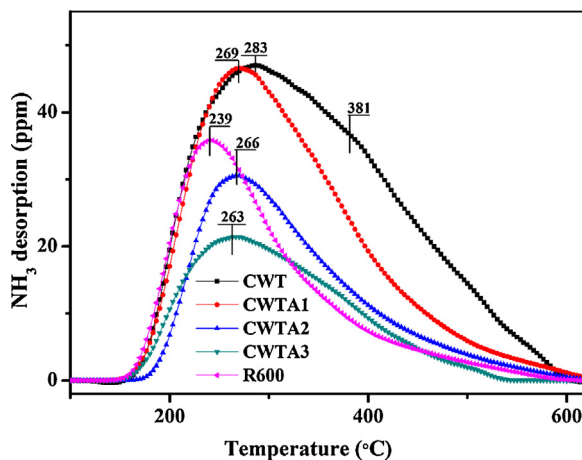


Fig. 7. NH_3 -TPD curves of the fresh, poisoned and regenerated CWT catalysts.

3.4. Surface acidity

Besides the redox property, surface acidity is another critical factor during the SCR process. Thus, the effect of the amount and strength of the acid on the fresh, poisoned and regenerated catalysts in NH_3 -TPD experiments is illustrated in Fig. 7. Two large ammonia desorption peaks observed at approximately $283\text{ }^\circ\text{C}$ and $381\text{ }^\circ\text{C}$, can be attributed to the weak and strong acid sites for the CWT catalysts. With increasing As loading, the intensity of high-temperature ammonia desorption peak of poisoned catalysts decreases gradually along with shifting low-temperature desorption peak position (toward low temperature). These results imply that the addition of As_2O_3 to CWT catalysts not only decreases the total amount of acid but influences the strength of the acid sites especially for strong acid sites, and these strong acid sites cannot recover after H_2 reduction regeneration in spite of successful reactivation weak acid sites as shown in Fig. 7.

In situ DRIFTS experiments are also employed to explore the NH_3 desorption behavior of the catalysts to further distinguish the different acid types. The NH_3 adsorption/desorption on the fresh and poisoned catalysts is shown in Fig. 8, and the regenerated catalyst is shown in Fig. S5. For fresh catalyst, the bands at 1280 and 1560 cm^{-1} can be assigned to the Lewis acid sites, whereas the band at 1440 and 1672 cm^{-1} can be attributed to the Brønsted acid sites [36]. Three small peaks on the broad band in the range $3150\text{--}3400\text{ cm}^{-1}$ are observed in the spectrum belong to contributions from ν_{as} (N-H), ν_{s} (N-H), $2\delta_{\text{as}}$ (H-N-H), $2\delta_{\text{s}}$ (H-N-H) and δ_{as} (H-N-H) modes of ammonia adsorbed on the

Lewis acid sites [37,38]. However, after poisoning by As_2O_3 , the peak at 1280 cm^{-1} decreases and the peak at 1560 cm^{-1} disappears, whereas the new characteristic peaks at 1612 cm^{-1} and at 1530 cm^{-1} (above $200\text{ }^\circ\text{C}$) corresponding to Lewis acid sites and amine species respectively produced by As species are observed, which were also found on deactivated commercial SCR catalyst by arsenic by other researchers [21]. In addition, the negative band centered at approximately 3679 cm^{-1} for both the two samples, ascribed to Ti-OH stretching frequencies, weakens and is partly replaced by a new peak at 3614 cm^{-1} , which is attributed to the As-OH stretching frequency [17,39]. To further investigate the changes of acid strength and amount at different temperatures, the Brønsted and Lewis acidities are obtained by integrating the areas in the DRIFTS spectra and normalized by the total acidity calculated by NH_3 -TPD results (Fig. 8c). As shown in the figure, the stability of Lewis acidity of the poisoned catalyst decrease more sharply than that of Brønsted acidity despite the transformation from Brønsted acid sites to Lewis acid sites occurring below $200\text{ }^\circ\text{C}$. And the slower lessened process of Brønsted acidity may arise from new Brønsted acid sites (As-OH) provided by As species. Peng et al. held that CeO_2 (on Ce^{3+}) mainly provided Lewis acid sites and that WO_x (with an appropriate doping amount) promoted the generation of Brønsted acid sites when studying the $\text{CeO}_2\text{-WO}_3$ catalyst [40]. Shan et al. attributed the Lewis acid sites to not only the CeO_2 but also the formation of unsaturated W_n^+ cations [15]. These results indicate that poisoning by As_2O_3 destroys the reaction active sites provided by CeO_2 and unsaturated W_n^+ cations, and thus significantly decrease the stability of Lewis acid sites as well as the amount of the Lewis and Brønsted acid sites.

3.5. $\text{NO} + \text{O}_2$ adsorption

Since the oxidation of NO to NO_2 may be the rate-determining step in the low-temperature SCR pointed by previous researchers, the NO_x adsorption properties over the fresh, CWT A3 and regenerated catalysts at $100\text{ }^\circ\text{C}$ are tested using in situ DRIFTS. As shown in Fig. 9, the bands centered at 1299 and 1482 cm^{-1} can be ascribed to the presence of bidentate nitrate and monodentate nitrate. And the bands at 1380 , 1517 and 1571 cm^{-1} are assigned to nitro compounds, bidentate nitrate and bridging nitrate respectively [8,41,42]. Finally, the band at 1601 cm^{-1} can be attributed to the adsorbed NO_2 [36]. After As_2O_3 introduced, the band corresponding to bridging nitrates shift to higher wavenumber (1578 cm^{-1}) and the nitro compounds and the adsorbed NO_2 decrease sharply; whereas the bidentate nitrate characteristic band (1299 cm^{-1}) can no longer be observed with new band at 1482 cm^{-1} appearance. These changes mean that part of NO_x adsorption sites of fresh cat-

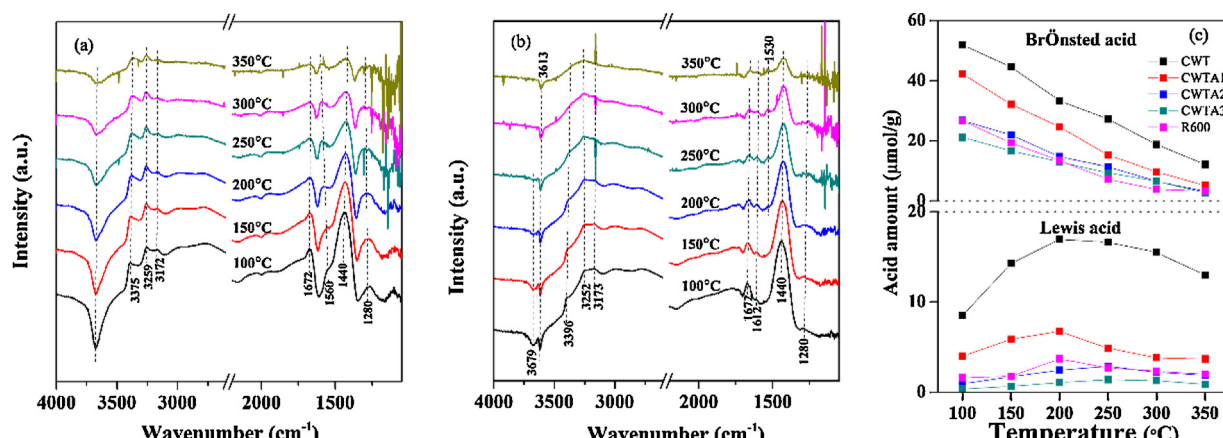


Fig. 8. DRIFTS spectra of the NH_3 desorption of the CWT (a) and CWT A3 (b) catalysts and the contributions of the Lewis and Brønsted acid sites over the fresh, poisoned and regenerated CWT catalysts.

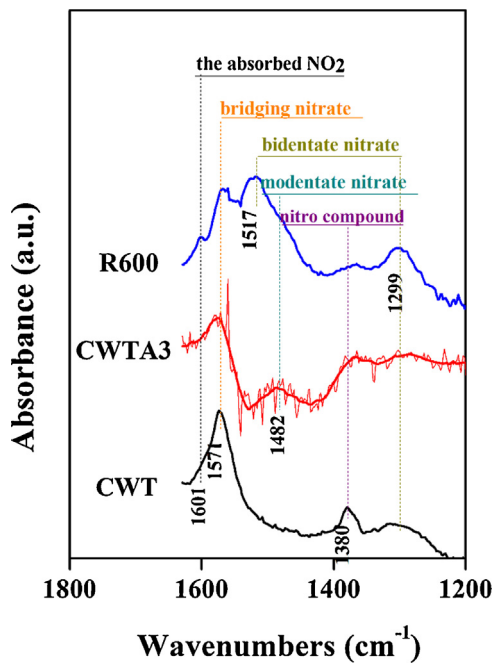


Fig. 9. DRIFTS spectra of the NO_x adsorption of the fresh, poisoned and regenerated CWT catalysts at 100°C .

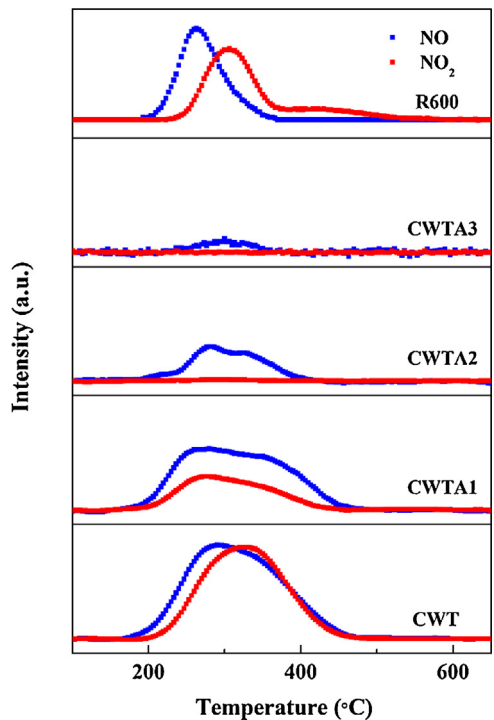


Fig. 10. $\text{NO} + \text{O}_2$ -TPD curves of the fresh, poisoned and regenerated CWT catalysts.

alysts are replaced by new ones that may be connected with As species. In addition, for regenerated catalysts, besides significant recovery of original NO_x adsorption sites, a new bidentate nitrate adsorption site at 1517 cm^{-1} occurs, which may be related with the $\text{Ce}_2(\text{WO}_4)_3$ species after high temperature reduction.

$\text{NO} + \text{O}_2$ -TPD experiments are also used to study the oxidation activity for the conversion of NO to NO_2 on the CWT series catalysts and the results are shown in Fig. 10. In the $\text{NO} + \text{O}_2$ desorption profiles of CWT, two NO desorption peaks are observed at 287 and 350°C as well as NO_2 desorption centered at 320°C . Both the

high temperature NO desorption peak and NO_2 one move toward low temperature direction with increasing As_2O_3 , which implies the capacity and stability of NO and NO_2 adsorption weaken. Moreover, the NO_2 desorption peak almost disappears for CWTa3. Because the desorption of NO_2 ascribed to the decomposition of the bound nitrate species, NO_x adsorption is greatly suppressed with As species introduced, which is consistent with in situ DRIFTS results. After regeneration, although the low temperature NO desorption peak and NO_2 desorption peak restore partly, the high temperature NO desorption peak hardly arise, which may be related with the weaker NO adsorption ability of $\text{Ce}_2(\text{WO}_4)_3$ species and fewer surface defect sites for R600.

3.6. Chemical states analysis (XPS)

In order to obtain surface information about the oxidation state of As and Ce cations over CWT series catalysts and to ensure the atomic concentrations of the surface layer, XPS spectra of the samples are recorded. The XPS spectra of As3d are shown in Fig. 11(a) and two peaks can be observed by fitting the curves. As reported in the previous literature, the peak centered at $44.7\text{--}45.1\text{ eV}$ can be assigned to As^{3+} and the one centered at approximate 45.9 eV corresponding to As^{5+} [43]. As shown in Fig. 11(a), only 23.85% As^{3+} species exist on the CWTa1 catalysts surface, and As^{5+} species decrease gradually to 58.92% despite the major body of arsenic with increasing the As_2O_3 loading content to 3%. Furthermore, the binding energy corresponding to As^{5+} moves to the direction of high energy, which clearly suggests the strong interaction between Ce(W) and As on the surface of TiO_2 exists. These results show difference with our previous article focused on As poisoned commercial VWTi catalysts, which described that As species was prefer to anchored onto the catalyst surface as an pentavalent arsenate (V) species at high content, conversely, As_2O_3 species as the main existing form at low As concentration.

The deconvoluted Ce3d XPS results of fresh, poisoned and regenerated catalysts are shown in Fig. 11(b). As can be seen from figure, the peaks denoted as “v” and as “u” correspond to $\text{Ce}3d_{5/2}$ spin-orbit components and $\text{Ce}3d_{3/2}$ spin-orbit components, respectively. The bands v , v' , v'' , u , u' , and u'' (blue color curves) can be attributed to surface Ce^{4+} species with $3d^{10}4f^0$ electronic state, whereas v' and u' (red color curves) can be ascribed to surface Ce^{3+} atoms corresponding to the $3d^{10}4f^1$ initial electronic configuration [44]. Based on previous reports, the superior percentages of Ce^{3+} on the surface of catalysts can generate a charge imbalance, oxygen vacancies and unsaturated chemical bonds over the catalyst surface to promote the NO oxidation reaction and to facilitate for the faster kinetics in SCR process [30,35]. However, as the As_2O_3 mass ratio increases to 3%, the value of surface Ce^{3+} atomic concentration (Table 2) drops to 1.29% with higher binding energy. These facts indicate that the surface charge imbalance and oxygen vacancies originating from surface Ce^{3+} species recede because of their surrounding As species stronger electron withdrawing ability, which makes part of surface cerium atoms maintain at the high-valence state.

The deconvoluted O1s XPS spectra for the investigated catalysts are presented in Fig. 11(c). As can be seen from the figure, all the samples show two distinct sub-bands. The O 1s binding energies located at around 528.9 eV can be ascribed to lattice oxygen O_2^- (designated as “ β ”); the binding energies at $531.1\text{--}531.5\text{ eV}$ belonging to surface labile oxygen such as defect-oxide O^- or hydroxyl-like group OH^- (labeled as “ α ”) [45,46]. The oxygen “ $\text{O}\beta$ ” may be primarily originated from $\text{Ti}-\text{O}$ in the anatase crystal lattice, and the oxygen “ $\text{O}\alpha$ ” can be attributed to the $\text{Ce}-\text{OH}$, $\text{W}-\text{OH}$ and $\text{Ti}-\text{OH}$ over the surface [47]. It has been well established in the previous literature that the surface chemisorbed labile oxygen ($\text{O}\alpha$) is more active than lattice oxygen because its higher mobility, and thus it always plays a key role in NO oxidation reactions at low tem-

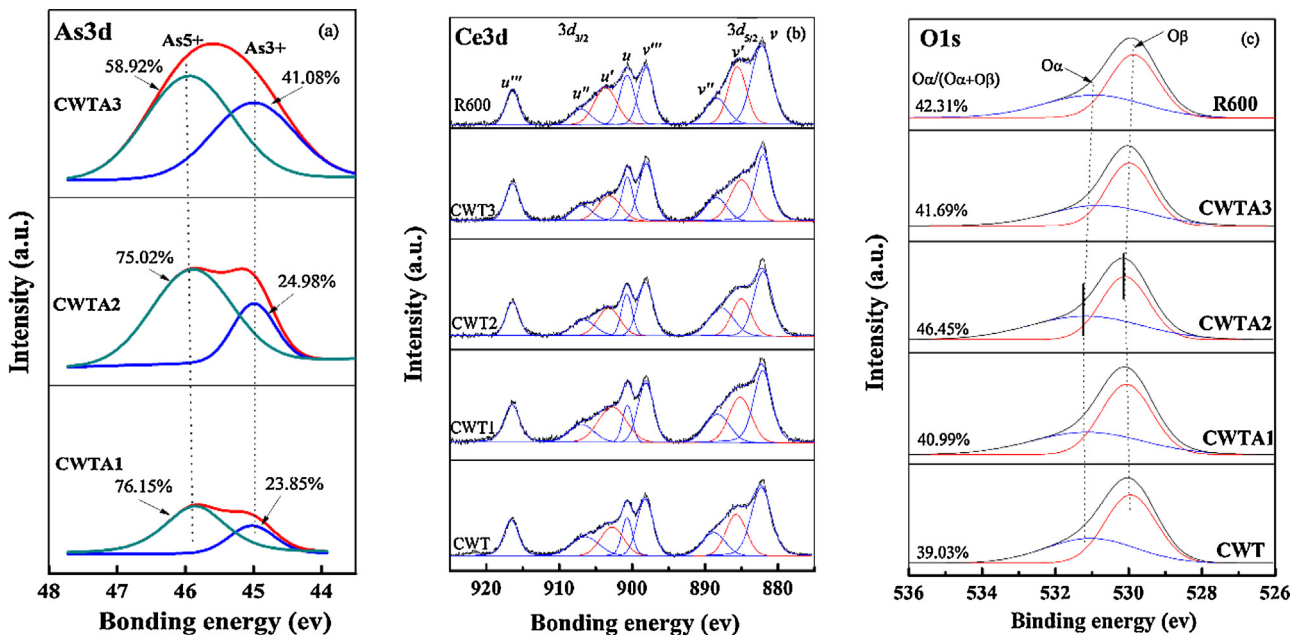


Fig. 11. XPS spectra of the fresh, poisoned and regenerated CWT catalysts over the spectral regions of As 3d (a), Ce 3d (b) and O 1s (c).

Table 2
XPS results of fresh, poisoned and regenerated catalysts.

Catalyst	Surface atomic concentration (%)										
	Ce ⁴⁺	Ce ³⁺	Ce _{total}	O _α	O _β	O _{total}	As ⁵⁺	As ³⁺	Astotal	W	Ti
CWT	6.04	2.01	8.06	27.45	42.89	70.34	—	—	—	4.4	17.21
CWT _{A1}	4.1	1.76	5.86	29.15	41.97	71.12	0.64	0.2	0.84	4.03	18.14
CWT _{A2}	3.49	1.4	4.89	33.2	38.27	71.47	1.16	0.39	1.55	3.72	18.37
CWT _{A3}	3.55	1.29	4.84	29.16	40.78	69.94	0.94	0.66	1.6	3.73	19.89
R600	4.52	1.89	6.41	30.3	41.31	71.61	—	—	0.15	3.92	17.91

perature [48,49]. Accordingly, the existence of high O_α/(O_α + O_β) ratio can facilitate the “fast SCR” reaction. The relative concentration ratios of O_α/(O_α + O_β) for each catalyst is also calculated and the results are shown in Fig. 11(c). It is clear that CWT_{A2}, not CWT, has the greatest amount of chemisorbed oxygen species among the catalysts, which is relate to the transformation from lattice oxygen under the effect of arsenic, and account for the much stronger oxidizability of the sample shown in H₂-TPR results. Additionally, it should be noted that, when the mass ratio of As₂O₃ is below 2%, there is almost no arsenic crystal phase can be seen in Fig. 1. Therefore, surface As–OH makes some contribution to the surface chemisorbed labile oxygen, whereas this contribution wears off with As content continue increase, on account of the As₂O₅ crystallized structure formation. The highest O_α bond energy of CWT_{A2} sample also hint the strong binding force given by surrounding As species introduced, which is not beneficial for low temperature NO oxidation reaction. Finally, although there is no good correlation between the SCR reactivity and the relative concentration ratios of O_α/(O_α + O_β), we can find that the O_α bond energy returns to the level of fresh catalysts after regeneration. These suggest H₂ reduction regeneration is a good method to remove the surface As species which constrains the surface labile oxygen.

3.7. Reactivity of surface-adsorbed species

Particular studies on the reactivity of surface-adsorbed NH₃ and NO_x species are carried out using in situ DRIFTS over the CWT series catalyst at 200 °C and 300 °C respectively, and spectra are recorded as a function of time (Fig. 12). Fig. 12(a) shows the DRIFTS

spectra of CWT catalyst in a flow of NO + O₂ after pretreated by a flow of NH₃ for 30 min and N₂ purging for 30 min at 200 °C. As illustrated in Fig. 12(a), when catalyst is treated with NH₃, coordinated NH₃ species (1089, 1302, and 1596 cm⁻¹), NH₄⁺ species (1441 and 1684 cm⁻¹) and NH stretching region bands (3164, 3264 and 3385 cm⁻¹) form on CWT surface [50]. After switching the gas to NO + O₂, all ammonia adspecies decrease and vanish in 20 min. Meanwhile, some new bands attributed to NO_x species appeared (1107, 1309, 1376 and 1584 cm⁻¹). These results indicate that both Lewis and Brønsted acid sites can participate in the SCR reaction with NO_x species at 200 °C. When the reactants are introduced to in situ cell in the reversed order, the bands of adsorbed NO₂ (1653 cm⁻¹) and nitro compounds (1375 cm⁻¹) vanish within 5 min after NH₃ purged. Meanwhile the intensity of the band at 1297 cm⁻¹ decreases firstly and then increases, which may be due to the bidentate nitrate species reaction and soon after overlap of the bands of coordinated NH₃ species. In addition, in spite of NH₃ existence, the intensity of the band at 1573 cm⁻¹ (bridging nitrate) almost remains with its position slight shifting to high wavenumber at 1578 cm⁻¹. The above results show that the NH₃ species bonded to the Brønsted and Lewis acid sites can participate in the SCR reaction with bidentate nitrate and adsorbed NO₂ species rather than monodate or bridging nitrates at low temperatures for fresh catalyst.

However, for poisoned catalyst (Fig. 12(b)), Lewis acid sites (1280 and 1604 cm⁻¹) significantly decrease and a new band at 1540 cm⁻¹ occurs after the catalyst exposed to NH₃. According to Ramis's proposal, this band may be related to the intermediate amide of excess oxidation of ammonia [51]. Moreover, when

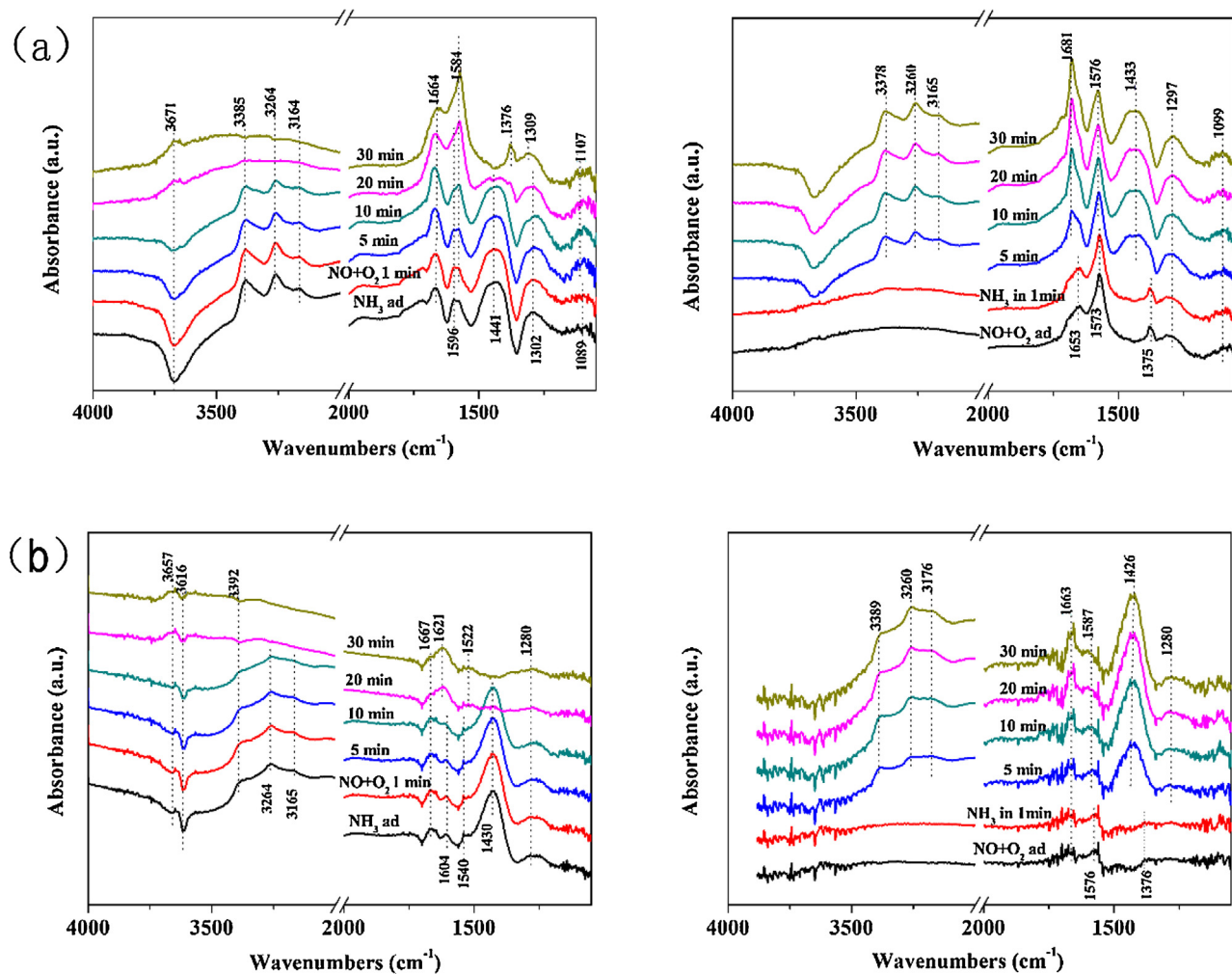


Fig. 12. Sequential DRIFTS spectra of CWT (a) and CWTA3 (b) recorded under various atmospheres: the dehydrated catalyst was first treated by NH_3 , then $\text{NO} + \text{O}_2$ was added and the reversed order at 200°C .

catalyst is purged by $\text{NO} + \text{O}_2$, the bands ascribed to adsorbed NO_2 (1620 cm^{-1}) and bidentate nitrate (1522 cm^{-1}) species appear gradually without Lewis acid sites vanishment. Furthermore, when the gaseous order is reversed, only few bands due to monodentate nitrate (1280 cm^{-1}) nitro compounds (1376 cm^{-1}), bridging nitrate (1576 cm^{-1}) and adsorbed NO_2 (1663 cm^{-1}) rather than reactable bidentate nitrate species can be observed after $\text{NO} + \text{O}_2$ adsorption. And these bands are soon covered by the adsorbed NH_3 . On the basis of the above results, it can be concluded that the absorption of Lewis acid sites and bidentate nitrate species is inhibited greatly due to As poisoning effect, which can participate the low-temperature SCR process as an important precursor for fresh catalyst. DRIFT spectra of regenerated catalyst is also recorded under the same reaction condition (Fig. S6). It is found that the adsorption of Lewis acid sites and bidentate nitrate species can be recovered. Besides that, a new band, not shown in fresh and poisoned catalysts, corresponding to new bidentate nitrate species can also participate in the low-temperature SCR reaction.

Fig. 13 presents the DRIFTS spectra of fresh, poisoned and regenerated catalyst in a flow of $\text{NO} + \text{O}_2$ after the catalyst was pre-exposed to NH_3 atmosphere for 30 min followed by N_2 purging at 300°C . When the fresh catalyst is exposed to NH_3 , all the coordinated NH_3 on the Lewis acid sites (1284 and 1601 cm^{-1}), NH_4^+ species (1417 and 1463 cm^{-1}) and NH stretching region bands (3165 , 3265 and 3377 cm^{-1}) can be detected, while only NH_4^+ species and a small peak at 1608 cm^{-1} assigned to bridging nitrate

that may be related to the NH_3 oxidation for poisoned catalyst. In addition, bidentate nitrate, NH_4NO_3 and monodentate nitrate species (1294 , 1368 and 1481 cm^{-1}) and H_2O (1618 cm^{-1}) as intermediates during SCR reaction emerge with adsorbed NH_3 species decreasing on CWT surface when NO and O_2 are introduced. Conversely, no chance happen for poisoned catalyst within 30 min after $\text{NO} + \text{O}_2$ introduced. When the gas order is reversed, the adsorbed NO_x species on fresh (more) and poisoned (few) catalyst surface vanish gradually when switching the gas to NH_3 . After 3 min, only the adsorbed NH_3 can be found in the DRIFT spectra (Fig. S7). These results imply that, even poisoned by As, bridging and monodentate nitrate species can also react with the adsorbed NH_3 at high temperature, nevertheless adsorbed and activated NH_3 rarely react with $\text{NO} + \text{O}_2$. Finally, the spectra of regenerated catalyst shows no difference with fresh one as shown in Fig. 13(c).

4. Discussions

4.1. The influence of the arsenic on the catalyst structure and active sites

Analysis of the structure of the As phase with different contents by XRD and Raman shows no evidence of As_2O_5 but peaks shift for CWTA1 and CWTA2, which suggest As phase is present as a surface species and exists strong interaction with surrounding Ce proved by in situ Raman results (Fig. 6). In addition, some As ions

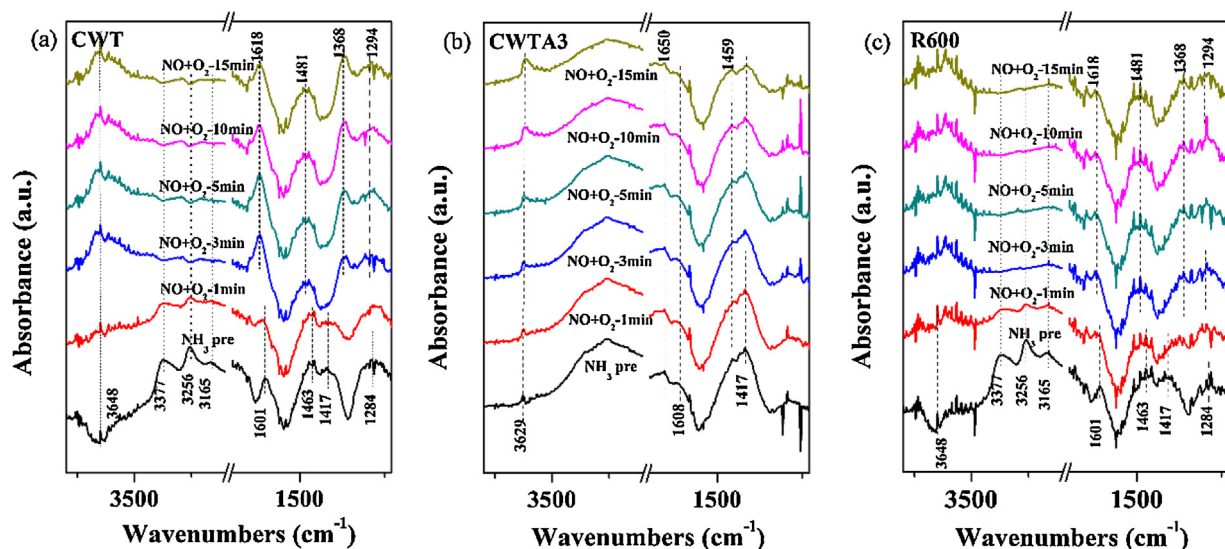
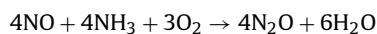


Fig. 13. Sequential DRIFTS spectra of CWT (a), CWTA3 (b) and R600 (c) recorded under atmospheres: the dehydrated catalyst was first treated by NH_3 , then $\text{NO} + \text{O}_2$ was added at 300°C .

can enter into the CeO_2 lattice as the radius of As^{3+} (0.058 nm) is less than that of Ce^{4+} (0.087 nm). For poisoned catalysts, substitution of a Ce^{4+} ion by As^{3+} in the CeO_2 network leads to a deficient electron which is adverse to the formation of a Ce^{3+} ion. Moreover, on account of higher electronegativity for As (2.18) than Ce (1.12), the surface concentration of Ce^{3+} species decrease gradually with increasing As content because of electron-withdrawing of As. However, these Ce^{3+} ions are crucial to the formation of oxygen vacancies and less bonded oxygen as it can result in charge imbalance and unsaturated chemical bonds. Furthermore, it is proven that facile Ce^{4+} to Ce^{3+} redox cycle as active sites can promote reducibility of these Ce sites that makes them more reactive in NH_3 -SCR reaction. Therefore, it means that the adjacent oxygen species around cerium sites and redox cycle of Ce sites are inhibited by As. On the other hand, as displayed in H_2 -TPR and XPS results, both the oxidizability and the $\text{O}_\alpha/(\text{O}_\alpha + \text{O}_\beta)$ concentration ratios of poisoned catalysts are enhanced, simultaneously, a new peak at 1540 cm^{-1} corresponding to intermediate NH_2^- can be found in the DRIFTS spectra results. Accordingly, N_2O production grows dramatically with decreasing NOx conversion. In fact, N_2O as the by-product of the NH_3 -SCR reaction goes through the non-selective catalytic reduction (NSCR) process:



Therefore, the more surface-active oxygen and stronger oxidizability provided by arsenic leads to strong NSCR and NH_3 oxidation, which is harmful to SCR process. When As_2O_3 mass ratio is added to 3%, unsaturated coordinated As species gather up, form crystallized structure and deposit on surface and in channel of catalysts with surface area and pore volume shrinking. That makes the strong reducing capacity (H_2 -TPR) and the reaction activity decrease further for CWTA3. In a word, depositional As_2O_5 leads to the SCR reactant gases may have few opportunities to diffuse into the Ce atoms and active oxygen species surface and thus lose activity further.

4.2. The influence of the arsenic on the reaction mechanism

The FTIR study of $\text{NO} + \text{O}_2$ adsorption shows that several adsorbed NOx species are identified in the DRIFT spectra of fresh and poisoned catalysts. On CWT, NO is supposed to be initially

adsorbed on basic $\text{Ce}-\text{O}^{2-}$ sites, and then oxidized to NO_3^- and NO_2 . However for CWTA3, the introduction of As species leads to the intensity of NOx adsorption weaken at temperatures below 200°C . Meanwhile, larger amount of new monodentate nitrate species corresponding to $\text{As}-\text{O}_2^-$ sites adsorption and oxidation form as shown in Fig. 12. However, it can be seen that this kind of monodentate nitrate species hardly participate in the NH_3 -SCR reaction on CWTA3 at low temperatures. Moreover, the number of coordinated NH_3 is much lower than NH_4^+ ions due to the effect of As. As a result, less coordinated NH_3 , reactable nitrates (NO_3^-) and adsorbed NO_2 depress the SCR reaction at low temperature. With the temperature continuous increase to 300°C , a large amount of nitrate species still exist steadily despite adsorption intensity decrease. But all the monodentate nitrate, bidentate nitrate and adsorbed NO_2 can take part in SCR reaction with adsorbed NH_3 . Unfortunately, when $\text{NO} + \text{O}_2$ is passed over the NH_3 -adsorbed CWTA3 catalyst at a high temperature of 300°C , both the Lewis and Brønsted acid sites keep stable and unchanged.

On one hand, in view of previous reports and our findings, NH_3 -SCR process of CWT may mainly follow Langmuir–Hinshelwood (L–H) mechanism at low temperature (below 200°C), since both the adsorbed nitrogen oxide and ammonia species can be active in SCR reaction [15,41]. While in consideration of the low participation of the adsorbed nitrate species, the SCR reaction at high temperature (over 300°C) may primarily undergo the Eley–Rideal (E–R) mechanism. In particular, the adsorbed NH_3 is firstly activated and oxidized to NH_2 , which will subsequently react with NO to form NH_2NO intermediate and finally generate N_2 and H_2O . On the other hand, although increasing part Brønsted acid sites, the As_2O_3 impregnation impedes the adsorption of ammonia on Lewis acid sites and the formation of bidentate nitrate species and adsorbed NO_2 , which are both important steps for L–H mechanism at low temperature. At high temperatures, the adsorbed NH_3 species hardly react with NO due to excess NH_3 oxidation even though the adsorbed NO_3^- still play a role in SCR reaction. In other words, because the major E–R process is inhibited, the high-temperature SCR reaction only follow minor L–H mechanism. In this way, both the low-temperature and high-temperature activity of poisoned catalysts is greatly depressed.

4.3. H_2 reduction regeneration mechanism of arsenic deactivated Ce-W/Ti catalysts

Simple H_2 reduction regeneration can make the activity of deep As poisoned catalysts recover to more than 80% no matter at low temperature or high temperature as shown in Fig. 4. Consequently, it is a better method for regeneration of As poisoned catalysts than H_2O_2 solution and alkaline $Ca(NO_3)_2$ cleaning fluid used in other reports [21,28]. But high temperature reduction affects the properties of catalyst in several aspects. First, after regeneration part of amorphous WO_3 and cubic CeO_2 can been transformed into the form of crystalline $Ce_2(WO_4)_3$, and that makes the pore structure change and surface area shrink. Second, the H_2 reduction peak of W species moves forward (low temperature direction), and concentration of surface active oxygen slightly increase for R600 sample. These results may play a role on N_2O production growth shown in Fig. 3(b), because of higher oxidizability in favor of NH_3 oxidation. Third, as pointed by previous researches, WO_3 as an important promoter, not only brings in many Brønsted acid sites, but also accelerates the NH_3 activation. But because of WO_3 structural changes after regeneration, strong acid sites vanish and thermal stability of remaining weak acid lower when compared with fresh sample. In addition, high temperature reduction can also do something good to the promotion of SCR reaction such as surface Ce^{3+}/Ce^{4+} ratio raise and new NO_x adsorptive sites forming.

In a word, although H_2 reduction regeneration partly changes the structure, reducibility and surface acidity, it can remove the As species from the catalyst surface effectively, and make poisoned one easily recover up to more than 80% initial activity. So it is a simple and efficient way for As poisoned catalyst regeneration.

5. Conclusions

Poisoning mechanism and regeneration of arsenic on Ce-W/Ti catalysts are studied and discussed in this work. Arsenic at low loading is present as amorphous and can enter into the CeO_2 lattice. While at high loading, they gather up, form crystallized structure and deposit on surface and in channel of catalysts. Moreover, As_2O_5 with high oxidability and more surface active oxygen species on the catalyst surface considerably increases the N_2O due to NH_3 oxidation and side reaction occurrence. Furthermore, As species not only reduce the surface area, the number of Lewis acid sites and the strength of strong acid sites but also inhibit the NO_x adsorption and activation. At low temperature, because of As introduction, the lower adsorbed nitrate species and Lewis acid sites limit the SCR process. By contrast, the adsorbed NH_3 species hardly react with NO, which hints the major E-R process is inhibited at high temperature.

High temperature H_2 reduction regeneration can recover up to more than 80% original activity from deep As poisoned catalyst. Although it affects the properties of catalyst in several aspects: crystalline $Ce_2(WO_4)_3$ forming, surface active oxygen species and Ce^{3+}/Ce^{4+} ratio raise and loss of Brønsted acid sites provided by WO_3 , it is still a simple and efficient way for As poisoned catalyst regeneration.

Acknowledgements

This work was financially supported by National Natural Science Foundation of China (21325731, 21407088 & 51478241), National High-Tech Research and Development (863) Program of China (2013AA065401 & 2013AA065304), and China Postdoctoral Science Foundation (2013M530643).

Appendix A. Supplementary data

Supplementary data associated with this article can be found, in the online version, at <http://dx.doi.org/10.1016/j.apcatb.2015.11.042>.

References

- [1] R. Burch, S. Scire, Selective catalytic reduction of nitric-oxide with ethane and methane on some metal exchanged ZSM-5 zeolites, *Appl. Catal. B* 3 (1994) 295–318.
- [2] G. Busca, L. Lietti, G. Ramis, F. Berti, Chemical and mechanistic aspects of the selective catalytic reduction of NO_x by ammonia over oxide catalysts: a review, *Appl. Catal. B* 18 (1998) 1–36.
- [3] C. Cristiani, M. Bellotto, P. Forzatti, F. Bregani, On the morphological properties of tungsta-titania de- NO_x ing catalysts, *J. Mater. Res.* 8 (1993) 2019–2025.
- [4] J.A. Martens, A. Cauvel, A. Francis, C. Hermans, F. Jayat, M. Remy, M. Keung, J. Lievens, P.A. Jacobs, NO_x abatement in exhaust from lean-burn combustion engines by reduction of NO_2 over silver-containing zeolite catalysts, *Angew. Chem. Int. Ed.* 37 (1998) 1901–1903.
- [5] N.Y. Topsoe, H. Topsoe, J.A. Dumesic, Vanadia–titania catalysts for selective catalytic reduction (SCR) of nitric-oxide by ammonia. I. Combined temperature-programmed in-situ FTIR and online mass-spectroscopy studies, *J. Catal.* 151 (1995) 226–240.
- [6] G.S. Qi, R.T. Yang, R. Chang, MnO_x-CeO_2 mixed oxides prepared by co-precipitation for selective catalytic reduction of NO with NH_3 at low temperatures, *Appl. Catal. B* 51 (2004) 93–106.
- [7] F. Li, Y.B. Zhang, D.H. Xiao, D.Q. Wang, X.Q. Pan, X.G. Yang, Hydrothermal method prepared Ce–P–O catalyst for the selective catalytic reduction of NO with NH_3 in a broad temperature range, *Chemcatchem* 2 (2010) 1416–1419.
- [8] P. Li, Y. Xin, Q. Li, Z. Wang, Z. Zhang, L. Zheng, Ce–Ti Amorphous oxides for selective catalytic reduction of NO with NH_3 : confirmation of Ce–O–Ti active sites, *Environ. Sci. Technol.* 46 (2012) 9600–9605.
- [9] L. Chen, J. Li, W. Ablikim, J. Wang, H. Chang, L. Ma, J. Xu, M. Ge, H. Arandian, CeO_2-WO_3 mixed oxides for the selective catalytic reduction of NO_x by NH_3 over a wide temperature range, *Catal. Lett.* 141 (2011) 1859–1864.
- [10] W. Shan, F. Liu, H. He, X. Shi, C. Zhang, Novel cerium–tungsten mixed oxide catalyst for the selective catalytic reduction of NO_x with NH_3 , *Chem. Commun.* 47 (2011) 8046–8048.
- [11] Y. Peng, R. Qu, X. Zhang, J. Li, The relationship between structure and activity of MoO_3-CeO_2 catalysts for NO removal: influences of acidity and reducibility, *Chem. Commun.* 49 (2013) 6215–6217.
- [12] R. Qu, X. Gao, K. Cen, J. Li, Relationship between structure and performance of a novel cerium–niobium binary oxide catalyst for selective catalytic reduction of NO with NH_3 , *Appl. Catal. B* 142 (2013) 290–297.
- [13] Z. Liu, Y. Yi, J. Li, S.I. Woo, B. Wang, X. Cao, Z. Li, A superior catalyst with dual redox cycles for the selective reduction of NO_x by ammonia, *Chem. Commun.* 49 (2013) 7726–7728.
- [14] Z. Liu, J. Zhu, J. Li, L. Ma, S.I. Woo, Novel Mn–Ce–Ti mixed-oxide catalyst for the selective catalytic reduction of NO_x with NH_3 , *ACS Appl. Mater. Interfaces* 6 (2014) 14500–14508.
- [15] W. Shan, F. Liu, H. He, X. Shi, C. Zhang, A superior Ce–W–Ti mixed oxide catalyst for the selective catalytic reduction of NO_x with NH_3 , *Appl. Catal. B* 115–116 (2012) 100–106.
- [16] C.L. Senior, D.O. Lignell, A.F. Sarofim, A. Mehta, Modeling arsenic partitioning in coal-fired power plants, *Combust. Flame* 147 (2006) 209–221.
- [17] F. Hilbrig, H.E. Göbel, H. Knözinger, H. Schmelz, B. Lengeler, Interaction of arsenious oxide with $DeNO_x$ -catalysts: an X-ray absorption and diffuse reflectance infrared spectroscopy study, *J. Catal.* 129 (1991) 168–176.
- [18] E. Hums, A catalytically highly-active, arsenic oxide resistant V–Mo–O phase—results of studying intermediates of the deactivation process of $V_2O_5-MoO_3-TiO_2$ (ANATASE) $DeNO_x$ catalysts, *Res. Chem. Intermed.* 19 (1993) 419–441.
- [19] Y. Peng, J. Li, W. Shi, J. Xu, J. Hao, Design strategies for development of SCR catalyst: improvement of alkali poisoning resistance and novel regeneration method, *Environ. Sci. Technol.* 46 (2012) 12623–12629.
- [20] Y. Peng, J. Li, L. Chen, J. Chen, J. Han, H. Zhang, W. Han, Alkali metal poisoning of a CeO_2-WO_3 catalyst used in the selective catalytic reduction of NO_x with NH_3 : an experimental and theoretical study, *Environ. Sci. Technol.* 46 (2012) 2864–2869.
- [21] Y. Peng, J. Li, W. Si, J. Luo, Y. Wang, J. Fu, X. Li, J. Crittenden, J. Hao, Deactivation and regeneration of a commercial SCR catalyst: comparison with alkali metals and arsenic, *Appl. Catal. B* 168–169 (2015) 195–202.
- [22] T. Ohsaka, F. Izumi, Y. Fujiki, Raman spectrum of anatase, TiO_2 , *J. Raman Spectrosc.* 7 (1978) 321–324.
- [23] X. Yao, Y. Xiong, W. Zou, L. Zhang, S. Wu, X. Dong, F. Gao, Y. Deng, C. Tang, Z. Chen, L. Dong, Y. Chen, Correlation between the physicochemical properties and catalytic performances of $Ce_xSn_{1-x}O_2$ mixed oxides for NO reduction by CO , *Appl. Catal. B* 144 (2014) 152–165.
- [24] J. Engweiler, J. Harf, A. Baiker, WO_x/TiO_2 catalysts prepared by grafting of tungsten alkoxides: morphological properties and catalytic behavior in the selective reduction of NO by NH_3 , *J. Catal.* 159 (1996) 259–269.

[25] A.S. Mamede, E. Payen, P. Grange, G. Poncelet, A. Ion, M. Alifanti, V.I. Pârvulescu, Characterization of WO_x/CeO_2 catalysts and their reactivity in the isomerization of hexane, *J. Catal.* 223 (2004) 1–12.

[26] A.S. Mamede, E. Payen, P. Granger, M. Florea, V.I. Pârvulescu, $\text{WO}_x\text{--CeO}_2$ and $\text{WO}_x\text{--Nb}_2\text{O}_5$ catalysts deactivation during hexane isomerization, *AIChE J.* 54 (2008) 1303–1312.

[27] K.S.W. Sing, Reporting physisorption data for gas/solid systems with special reference to the determination of surface area and porosity (Recommendations 1984), *Pure Appl. Chem.* 57 (1985) 603–619.

[28] X. Li, J. Li, Y. Peng, W. Si, X. He, J. Hao, Regeneration of commercial SCR catalysts: probing the existing forms of arsenic oxide, *Environ. Sci. Technol.* 49 (2015) 9971–9978.

[29] Y. Peng, J. Li, W. Si, J. Luo, Q. Dai, X. Luo, X. Liu, J. Hao, New insight into deactivation of commercial SCR catalyst by arsenic: an experiment and DFT study, *Environ. Sci. Technol.* 48 (2014) 13895–13900.

[30] T. Boningari, P.R. Ettireddy, A. Somogyvari, Y. Liu, A. Vorontsov, C.A. McDonald, P.G. Smirniotis, Influence of elevated surface texture hydrated titania on Ce-doped Mn/TiO₂ catalysts for the low-temperature SCR of NO_x under oxygen-rich conditions, *J. Catal.* 325 (2015) 145–155.

[31] M.A. Reich, M. Maciejewski, A. Bajer, Characterization by temperature programmed reduction, *Catal. Today* 56 (2000) 347–355.

[32] N.W. Hurst, S.J. Gentry, A. Jones, B.D. McNicol, Temperature programmed reduction, *Catal. Rev. Sci. Eng.* 24 (1982) 233–309.

[33] A. Trovarelli, C. Deleitenburg, G. Dolcetti, J.L. Lorca, CO₂ methanation under transient and steady-state conditions over Rh/CeO₂ and CeO₂-promoted Rh/SiO₂: the role of surface and bulk ceria, *J. Catal.* 151 (1995) 111–124.

[34] M.F.L. Johnson, J. Mooi, Cerium dioxide crystallite sizes by temperature-programmed reduction, *J. Catal.* 103 (2) (1987) 502–505.

[35] T. Zhang, R. Qu, W. Su, J. Li, A novel Ce-Ta mixed oxide catalyst for the selective catalytic reduction of NO_x with NH₃, *Appl. Catal. B* 176–177 (2015) 338–346.

[36] K.I. Hadjiivanov, Identification of neutral and charged N_xO_y surface species by IR spectroscopy, *Catal. Rev.* 42 (2000) 71–144.

[37] M.A. Centeno, I. Carrizosa, J.A. Odriozola, NO–NH₃ coadsorption on vanadia/titania catalysts: determination of the reduction degree of vanadium, *Appl. Catal. B* 29 (2001) 307–314.

[38] A.S. Mamede, E. Payen, P. Grange, G. Poncelet, A. Ion, M. Alifanti, V.I. Pârvulescu, characterization of WO_x/CeO_2 catalysts and their reactivity in the isomerization of hexane, *J. Catal.* 223 (2004) 1–12.

[39] F.C. Lange, H. Schmelz, H. Knözinger, Infrared-spectroscopic investigations of selective catalytic reduction catalysts poisoned with arsenic oxide, *Appl. Catal. B* 8 (1996) 245–265.

[40] Y. Peng, K. Li, J. Li, Identification of the active sites on CeO₂–WO₃ catalysts for SCR of NO_x with NH₃: an in situ IR and Raman spectroscopy study, *Appl. Catal. B* 140–141 (2013) 483–492.

[41] L. Chen, J. Li, M. Ge, DRIFT study on cerium–tungsten/titania catalyst for selective catalytic reduction of NO_x with NH₃, *Environ. Sci. Technol.* 44 (2010) 9590–9596.

[42] Z. Ma, X. Wu, Z. Si, D. Weng, J. Ma, T. Xu, Impacts of niobia loading on active sites and surface acidity in $\text{NbO}_x/\text{CeO}_2\text{--ZrO}_2\text{--NH}_3$ –SCR catalysts, *Appl. Catal. B* 179 (2015) 380–394.

[43] F. Lange, H. Schmelz, H. Knözinger, An X-ray photoelectron spectroscopy study of oxides of arsenic supported on TiO₂, *J. Electron. Spectrosc. Relat. Phenom.* 57 (1991) 307–315.

[44] S. Zhang, Q. Zhong, Y. Shen, L. Zhu, J. Ding, New insight into the promoting role of process on the CeO₂–WO₃/TiO₂ catalyst for NO reduction with NH₃ at low-temperature, *J. Colloid Interface Sci.* 448 (2015) 417–426.

[45] T. Gu, Y. Liu, X. Weng, H. Wang, Z. Wu, The enhanced performance of ceria with surface sulfation for selective catalytic reduction of NO by NH₃, *Catal. Commun.* 12 (2010) 310–313.

[46] Z. Wu, Z. Sheng, Y. Liu, H. Wang, J. Mo, Deactivation mechanism of PtO_x/TiO₂ photocatalyst towards the oxidation of NO in gas phase, *J. Hazard. Mater.* 185 (2011) 1053–1058.

[47] X. Li, J. Li, Y. Peng, T. Zhang, S. Liu, J. Hao, Selective catalytic reduction of NO with NH₃ over novel iron-tungsten mixed oxide catalyst in a broad temperature range, *Catal. Sci. Technol.* 5 (2015) 4556–4564.

[48] M. Kang, E.D. Park, J.M. Kim, J.E. Yie, Manganese oxide catalysts for NO_x reduction with NH₃ at low temperatures, *Appl. Catal. A* 327 (2007) 261–269.

[49] L. Chen, J. Li, M. Ge, Promotional effect of Ce-doped V₂O₅–WO₃/TiO₂ with low vanadium loadings for selective catalytic reduction of NO_x by NH₃, *J. Phys. Chem. C* 113 (2009) 21177–21184.

[50] D.R. Sellick, A. Aranda, T. García, J.M. López, B. Solsona, A.M. Mastral, D.J. Morgan, A.F. Carley, S.H. Taylor, Influence of the preparation method on the activity of ceria zirconia mixed oxides for naphthalene total oxidation, *Appl. Catal. B* 132–133 (2013) 98–106.

[51] G. Ramis, L. Yi, G. Busca, M. Turco, E. Kotur, R.J. Willey, Adsorption, activation, and oxidation of ammonia over SCR catalysts, *J. Catal.* 157 (1995) 523–535.